

Collisions between supercooled excitons in Cu₂O studied by time-resolved Lyman spectroscopyTakeshi Tayagaki,¹ Andre Mysyrowicz,² and Makoto Kuwata-Gonokami^{1,*}¹*Department of Applied Physics, The University of Tokyo and Solution Oriented Research for Science and Technology (SORST) JST, 7-3-1 Hongo, Bunkyo-ku, Tokyo 113-8656, Japan*²*Laboratoire d'Optique Appliquée, ENSTA, Ecole Polytechnique, Palaiseau, France*

(Received 10 May 2006; revised manuscript received 6 October 2006; published 29 December 2006)

Supercooled orthoexcitons are generated in Cu₂O by resonant two-photon excitation with a femtosecond laser pulse. The excitonic Lyman series is systematically analyzed by time-resolved induced-absorption measurements. The decay time of orthoexcitons as well as the buildup and decay times of paraexcitons are found to be dependent on their respective densities. With these results, the two-body excitonic spin-exchange and the exciton dissociation processes are investigated. The collision-induced spin-exchange process is found to dominate in the early stage of photoexcitation. The conditions required to obtain a Bose-Einstein condensate with paraexcitons are discussed.

DOI: [10.1103/PhysRevB.74.245127](https://doi.org/10.1103/PhysRevB.74.245127)

PACS number(s): 71.35.Lk, 71.35.Cc, 78.47.+p

I. INTRODUCTION

The exciton, which is an elementary electronic excitation of a semiconductor, can be viewed as a quasiparticle with a hydrogenlike internal energy level structure. Since this composite particle consists of two fermions, exciton ensembles can be described with Bose statistics. Due to their light mass, it may be possible with excitons to reach a Bose-Einstein condensation phase at a relatively high temperature.¹ Although much work has been devoted to this subject, experimental evidence of a Bose-Einstein condensation (BEC) of excitons is still controversial.² One key question related to this issue is the stability of excitons at the high densities required for BEC. To resolve this question, the details of the interactions between the excitons must be evaluated and the relaxation processes at a high density regime must be understood.

It was known for many years that excitons in cuprous oxide (Cu₂O) are unique candidates for the experimental demonstration of BEC.³ Yellow excitons are a textbook example of Wannier excitons with a hydrogenlike energy structure. The electronic dipole transition between the crystal ground state and the 1s excitonic state is forbidden by the parity selection rule and consequently the 1s excitonic state has a long radiative recombination lifetime. The effective mass of the 1s exciton in Cu₂O is approximately 3m_e, which yields a critical temperature of 2 K at an exciton density of 10¹⁷ cm⁻³. Because of their small exciton Bohr radius (*a*_B ~ 0.8 nm), excitons are expected to remain stable even at such a high density.

Due to electron-hole exchange, the fourfold degenerate 1s excitonic state is split into a threefold orthoexciton and a lower lying singlet paraexciton, with an energy splitting Δ*E*_{ortho-para} = 12 meV. The optical transition between the ground state and the paraexciton is strictly forbidden because the paraexciton is a pure spin-triplet state⁴ and the optical transition requires a spin-flip. As a consequence, the radiative lifetime of paraexcitons is extremely long, exceeding 1 microsecond in good quality samples. Furthermore, it is known that paraexcitons at low densities can be formed directly from orthoexcitons via a relaxation process involv-

ing an electron spin-flip and the interaction of an acoustic phonon.⁵ For these reasons, paraexcitons have been considered the best candidate for observing an excitonic BEC under thermal equilibrium conditions. However, the fundamental properties and dynamics of paraexcitons are still not well understood. This is due to the fact that the detection of paraexcitons by the most commonly used method so far, luminescence spectroscopy, is very difficult owing to its extremely weak radiative recombination probability.

An important question that must be resolved to confirm the possibility of obtaining an excitonic BEC condensate is the nature of the recombination channels appearing due to collisions at a high exciton density. Is the number of particles conserved during the collisions? Are the collisions accompanied by a raise of the excitonic temperature? A nonradiative decay process that has often been mentioned and discussed in the literature is the total Auger process, in which the internal energy of one exciton is transferred to another during a collision, thereby creating an electron and hole with very high kinetic energies. From a study of the phonon-side band emission of orthoexcitons, O'Hara *et al.*⁶ have come to the conclusion that the collision cross section of this total Auger recombination process is as large as *A* = 7 × 10⁻¹⁷ cm³/ns. This process is also effective for paraexcitons and consequently could prevent the reach of a critical density. On the other hand, Jolk *et al.*⁷ have claimed, based on a pump-probe measurements involving the higher Rydberg series in the visible region (*np* series), that the Auger coefficient is much smaller than *A* = 10⁻¹⁷ cm³/ns. A theoretical calculation also indicates that the Auger coefficient should be smaller than *A* = 10⁻²⁰ cm³/ns.⁸ More recently, Jang *et al.*⁹ have proposed another mechanism for the decay of excitons at high density, based on the formation of biexcitons. However, there is no experimental evidence for biexciton formation.

Kavoulakis and Mysyrowicz¹⁰ have also proposed a collision-induced spin-flip mechanism as a possible mechanism to explain the dissociation of orthoexcitons in a high-density regime. In their theoretical model, the two colliding orthoexcitons with a relative electron singlet spin configuration are converted into two paraexcitons without particle loss. The collision rate for this spin-exchange mechanism has

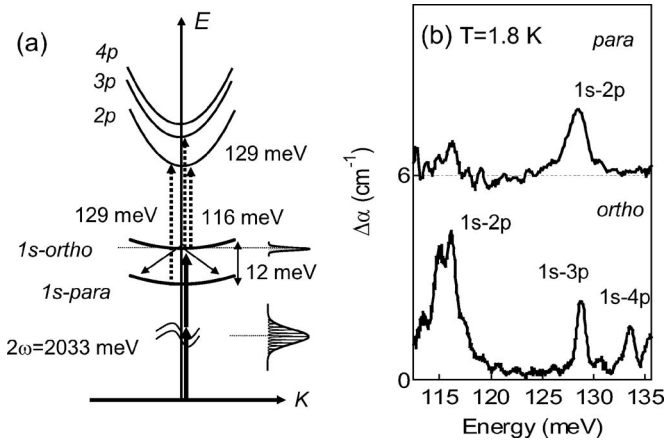


FIG. 1. (a) Schematic energy diagram of exciton Lyman series spectroscopy. (b) Lyman series spectra of orthoexcitons (lower curve) and $1s-2p$ line of paraexcitons (upper curve) for $T=1.8$ K, measured at 20 ps and 4 ns pump-probe delays, respectively.

been estimated to be larger than the Auger nonradiative recombination process.

The main experimental difficulty encountered to assess the relative importance of these processes lies in the measurement of the density of paraexcitons. An evaluation of the number of excitons and electron-hole pairs based on the luminescence intensity is problematic for the reasons discussed above (low luminescence efficiency). Recently, a much more promising method has been proposed in which the transition from the occupied $n=1$ level to higher terms of the series and continuum band is detected (exciton Lyman spectroscopy). Since the strength of the transition is directly proportional to the exciton density in the $n=1$ state (irrespective of the exciton species para or ortho) and to the transition matrix element, exciton Lyman spectroscopy is a powerful method to evaluate the exciton density for both orthoexcitons and paraexcitons precisely. In contrast to most other semiconductors, for which Lyman spectroscopy requires a detection in the far-infrared spectral range,^{11,12} the internal transitions of excitons in Cu_2O appear in the midinfrared^{13–15} because of the large excitonic binding energy. We have recently demonstrated a time-resolved midinfrared spectroscopy method,^{16,17} or time-resolved excitonic Lyman spectroscopy, which has allowed us to observe the temporal evolution of the density and the distribution in the momentum space of the orthoexcitons and paraexcitons in Cu_2O .

Figure 1(a) shows a schematic diagram of the excitonic Lyman spectroscopy method. In our study, the phase space compression scheme¹⁸ is used for the creation of an ultracold initial excitonic ensemble. The two-photon transition with a femtosecond laser pulse can create an initial population directly into a highly degenerate quantum state of cold orthoexcitons.^{17,19,20} We then probe the $1s-2p$ transitions of the orthoexcitons (116 meV) and paraexcitons (129 meV). Figure 1(b) shows the induced-absorption spectra measured at pump-probe delays of 20 ps and 4 ns. Comparing the spectra at the two delays, one notices that the $1s-2p$ signal of the orthoexcitons is weaker after 4 ns while the paraexciton $1s-2p$ signal becomes pronounced. We can distinguish the

$1s-2p$ transitions of orthoexcitons [lower part of Fig. 1(b)] and paraexcitons [upper part of Fig. 1(b)] because of the large exchange interaction which removes the ortho-para degeneracy. With such spectra, we could evaluate the temporal evolution of paraexcitons and observed an efficient orthoexciton to paraexciton transformation.¹⁹ In this analysis, we neglected the contribution of the $1s-3p$ orthoexciton signal, or the Lyman- β line from the $1s$ -ortho state, which overlaps with the $1s-2p$ paraexciton signal. In our latest experiments where the spectral resolution is enhanced, we obtained quantitative information about the wave function of the $1s$ exciton state and found a significant contribution from the Lyman- β line of $1s$ -orthoexciton states. In this paper, we present an improved analysis of time-resolved induced-absorption spectra in order to extract the temporal evolution of orthoexcitons and paraexcitons and to obtain information on the collision effects of excitons, such as the spin-flip processes and the dissociation processes. The feasibility of the spontaneous Bose-Einstein condensation of paraexcitons in Cu_2O following the loading of the supercooled $1s$ orthoexciton created by the resonant two-photon excitation is also discussed.

II. EXPERIMENT

A detailed description on the experimental method is given in previous papers by our group.^{13,19,16,17} A pulsed laser source of nearly transform-limited pulses around 1220 nm with a pulse width of 500 fs (8 nm spectral width), which is shaped from a 100 fs pulse by grating pairs, provides the pump pulse. This excitation pulse with an energy of 2.5 μJ is focused to an area of $2 \times 10^4 \mu\text{m}^2$ on the sample surface. The polarization of the excitation light is set to maximize the two-photon absorption coefficient. The 220 μm thick single crystal cut along the (100) plane is cooled by contact with a copper block maintained at liquid helium temperature. A tunable probe source in the midinfrared with a wavelength around 10 μm provides the weak probe pulse. The probe light is analyzed by a monochromator (resolution ~ 0.1 meV) followed by a HgCdTe detector. The Cu_2O crystal shows a suitable transparency window between 113 and 137 meV, allowing the observation of the transitions from the $1s$ orthoexciton to the np states and the $1s$ paraexciton to the $2p$ state.

III. RESULTS AND DISCUSSIONS

Figure 2(a) shows the temporal evolution of the Lyman series spectra under a low-power excitation with an initial orthoexciton density of $n \sim 0.8 \times 10^{15} \text{ cm}^{-3}$. The density of initial excitons is evaluated with the procedure reported in a previous paper.¹⁷ The $1s$ exciton density n_{1s} is related to the integrated area of the $1s-2p$ exciton absorption line, S_{1s-2p} , and can be expressed as

$$n_{1s} = \frac{\hbar c \sqrt{\epsilon}}{4\pi^2 E_{1s-2p} |\mu_{1s-2p}|^2} S_{1s-2p}, \quad (1)$$

where E_{1s-2p} , μ_{1s-2p} and ϵ are the $1s-2p$ transition energy, dipole moment and dielectric constant of linear response at the probe frequency. The $1s-2p$ transition dipole moment is

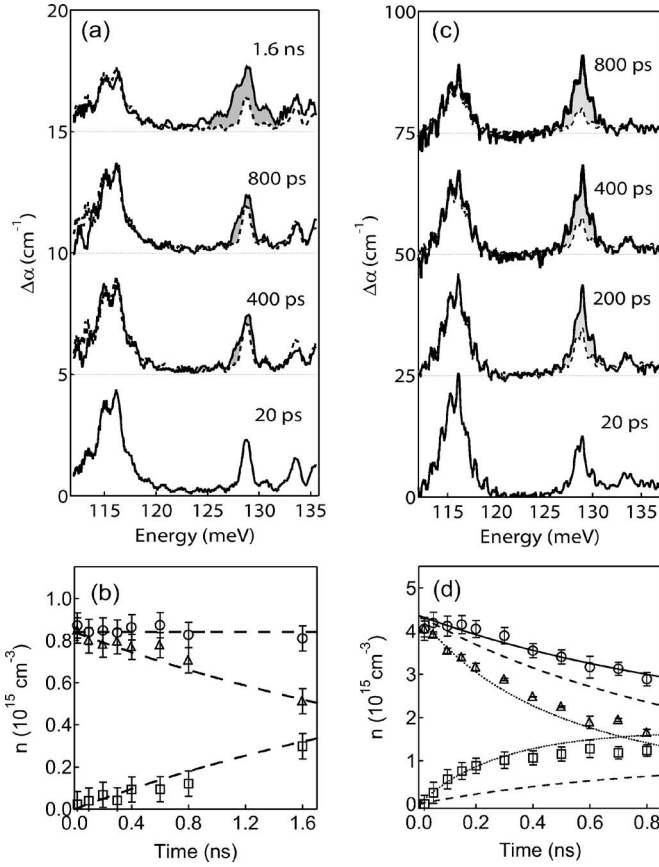


FIG. 2. (a) Temporal evolution of Lyman series spectrum under low-density excitation condition measured at 1.8 K. The hatched areas show the absorption of the $1s-2p$ transition of paraexcitons. (b) Temporal evolution of ortho (Δ), para (\square), and total (\circ) exciton density extracted from (a). The broken line shows the theoretical model with the linear relaxation from orthoexcitons to paraexcitons only. (c) Temporal evolution of Lyman series spectrum under high-density excitation condition. (d) Temporal evolution of ortho (Δ), para (\square), and total (\circ) exciton density extracted from (c). Calculated temporal evolution of the exciton densities with (dotted) and without (broken) the collision-induced spin-flip process $C=2.6 \times 10^{-16}$ cm³/ns, based on the model shown in Eqs. (3) and (4) with $A=10^{-16}$ cm³/ns.

estimated from the relative absorption strength of the $1s-np$ excitonic internal level transition, or Lyman series absorption, S_{1s-np}/S_{1s-2p} ($n=3,4$) under the assumption that the wave function of the excitonic ground state is well approximated by a modified $1s$ function of the hydrogenic model.⁴ The value found is $\mu_{1s-2p}=4.2e \text{ \AA}$. This provides a relation between the induced-absorption area and exciton density, $n_{1s}/S_{1s-2p}=6 \times 10^{13} \text{ cm}^{-3}/(\text{meV cm}^{-1})$.¹⁷

Induced-absorption lines at 116, 129, 133, and 136 meV are observed after a 20 ps pump-probe delay. These lines are assigned to the transition from the $1s$ to np states of the orthoexciton Lyman series.¹⁷ At a longer pump-probe delay, the induced-absorption lines of the orthoexciton decrease and the $1s-2p$ transition of the paraexciton appears 12 meV above the energy position of the $1s-2p$ orthoexciton transition. As shown in Fig. 1(b), there is a fortuitous overlap of the energy position corresponding to the $1s-2p$ transition of

paraexcitons and the $1s-3p$ orthoexcitons. In our previous paper,¹⁹ we neglected the contribution from the $1s-3p$ orthoexciton which led to an overestimate of the density of paraexcitons. Unfortunately, an estimate of the dipole moment of the paraexciton based on an analysis of the relative absorption strength of the higher terms of the Lyman series of paraexcitons is not possible because their energy positions are out of the transparency window of the crystal. To estimate the relative strength of the two components $1s-2p$ paraexcitons and $1s-3p$ orthoexcitons, we proceed as follows. We assume that the dipole moment of the paraexciton is the same as that of the orthoexciton. Since the direct optical excitation of paraexciton is forbidden by the selection rule, only the orthoexciton should exist just after the optical excitation. Therefore the Lyman series spectrum at a very early stage comes from the orthoexcitons only. The induced-absorption series of the orthoexciton, measured at a 20 ps pump-probe delay, is normalized by that of the $1s-2p$ transition as shown by the broken lines in Fig. 2(a). The integrated absorption of the paraexciton $1s-2p$ is estimated by subtracting the $1s-3p$ transition from the induced absorption around 130 meV [hatched area in Fig. 2(a)].

Figure 2(b) shows the temporal evolution of the orthoexciton and paraexciton density extracted from the results shown in Fig. 2(a) in the case of a low-density regime ($n < 10^{15} \text{ cm}^{-3}$). We note that during the first 2 ns, the orthoexciton decreases and the paraexciton increases, indicating the transformation of orthoexcitons into paraexcitons. We also note that the total number of excitons is approximately conserved during this time interval. The broken line in Fig. 2(b) shows the temporal evolution of the exciton densities using the ortho-para transformation rate $\Gamma_{o-p}=(3 \text{ ns})^{-1}$ obtained from the time-resolved luminescence measurement.⁵

The line shape of the Lyman spectrum reflects the excitonic distribution in the momentum space, which enables us to deduce the effective temperature of the excitons. By using the $1s-4p$ orthoexciton line, which has a narrow linewidth and no overlap with the paraexciton lines, we estimate the distribution in momentum space and the effective temperature of the excitons. Figure 3(a) shows the temporal evolution of the $1s-4p$ line of orthoexcitons measured at 4.2 K. To obtain the effective temperature of $1s$ orthoexcitons, we assume a Boltzmann distribution function because the density of the $1s$ orthoexcitons is less than 10^{15} cm^{-3} . The induced-absorption spectra $\Delta\alpha(E)$ as a function of the temperature of the excitons T is given by

$$\Delta\alpha(E) = \sqrt{E - E_{1s-4p}} \exp\left(\frac{-(E - E_{1s-4p})}{\left(\frac{m_{1s}}{m_{4p}} - 1\right)k_B T}\right), \quad (2)$$

where the effective mass of the $1s$ and $4p$ states are $m_{1s}=2.7m_e$ (Ref. 21) and $m_{4p}=1.7m_e$,²² and the $1s-4p$ transition energy is $E_{1s-4p}=133.4 \text{ meV}$. We neglect the intrinsic linewidth of the $1s$ exciton state which is much narrower ($\gamma_{1s} \ll 0.1 \text{ meV}$) than the spectral resolution of the present experiment. The linewidth of the $4p$ state with $\gamma_{4p}=0.6 \text{ meV}$ is used in our analysis. The bold lines in Fig. 3(a) show the results obtained from a curve fitting of the $1s-4p$ absorption

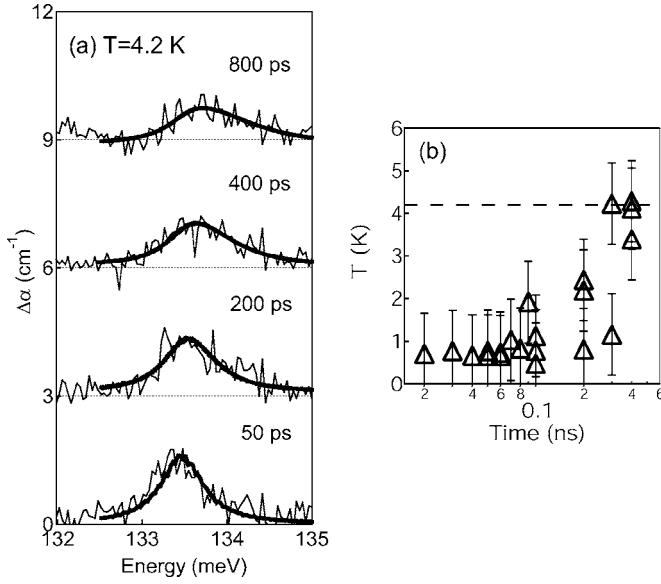


FIG. 3. (a) Temporal evolution of the $1s$ - $4p$ lines measured at 4.2 K. The bold lines show the fitting results of the $1s$ - $4p$ absorption lines. (b) Temporal evolution of the effective temperature of orthoexcitons extracted from (a). The horizontal dotted line shows the bath temperature ($T=4.2$ K).

lines. Although recent high-resolution spectroscopy measurements have revealed the anisotropy of the mass of orthoexcitons,²³ we used an isotropic, averaged mass for simplicity.

Figure 3(b) shows the extracted temporal evolution of the effective temperature of the exciton systems. As mentioned before, $1s$ orthoexcitons are initially in a supercooled state, where the temperature of the excitons is much lower than that of the lattice.¹⁷ The temperature of excitons increases gradually to the lattice temperature (4.2 K) in a 1 ns time interval. It has been argued previously from time-resolved luminescence measurements²⁴ that under low-density excitation the excitons form a thermal equilibrium with the lattice within a few hundred ps via LA phonon scattering process. This rate is a little higher than a theoretical calculation based on the known deformation potential of Cu_2O .²⁵

Figure 2(c) shows the temporal evolution of the Lyman series spectra under a high-density excitation ($\sim 4 \times 10^{15} \text{ cm}^{-3}$). The linewidth of the $1s$ - $4p$ line is slightly broader than the linewidth measured under a low-density excitation. The broadening of the $1s$ - $4p$ line occurs without a shift in the line position. Therefore, the broadening is not due to a temperature increment but to the Coulomb screening effect between the final np state and the $1s$ state. A similar effect was detected in a pump-probe experiment of the higher Rydberg series in the visible region (np series) by Mysyrowicz *et al.*²⁶ and Jolk *et al.*²⁷ In our experiments, no broadening is seen for the $1s$ - $2p$ line of the orthoexcitons, while slight broadening effects are observed in the higher $1s$ - np lines ($n=3,4$). Since the ratio of the absorption strength between the $1s$ - $2p$ and $1s$ - $4p$ transitions is almost entirely conserved, we assume that the relative strength of the $1s$ - $3p$ line is also conserved and subtract the contribution of $1s$ - $3p$ orthoexciton transition from the induced absorption

area of $1s$ - $2p$ paraexciton signal. With such an analysis we obtain the exciton density of both orthoexcitons and paraexcitons from the $1s$ - $2p$ transitions at various time delays. However, a further increase of the broadening at a higher-density excitation prevents us from distinguishing the peak structure of the $1s$ - np series at higher densities.

Figure 2(d) shows the temporal evolution of extracted exciton densities obtained using the procedure described above. At an early pump-probe delay ($t < 300$ ps), the nonlinear generation process of paraexcitons is more rapid than the linear orthoexciton-to-paraexciton conversion process. At a longer pump-probe delay ($t > 300$ ps), we observe a decrease of the total exciton density. The total exciton density decay rate is approximately proportional to the exciton density. This result indicates the presence of a two-body collision-induced decay. Detailed processes on the collision-induced decay and the redistribution have not yet been clarified. For simplicity and due to the lack of a better terminology, we adopt the usual terminology and call it an Auger recombination.

In order to discuss our results, the temporal evolution of the orthoexcitons n_o and paraexciton n_p are considered with the following model:

$$\frac{d}{dt}n_o = -\Gamma_{o-p}n_o - 2An_on_t + \frac{3}{4}An_t^2 - Cn_o^2, \quad (3)$$

$$\frac{d}{dt}n_p = \Gamma_{o-p}n_o - 2An_pn_t + \frac{1}{4}An_t^2 + Cn_o^2, \quad (4)$$

where $n_t (= n_o + n_p)$, Γ_{o-p} , A , C are the total exciton density, the transition rate from orthoexcitons-to-paraexcitons via phonon scattering and the cross sections of the collision-induced dissipation Auger and of the spin-flip process, respectively. We neglect the radiative recombination process because our experiment focuses on the fast dynamics of excitons in a nanosecond timeframe. For the collision-induced dissociation, we assume an Auger recombination model where the collision coefficients between the ortho-ortho A_{oo} , ortho-para A_{op} , and para-para excitons A_{pp} are identical, $A = A_{oo} = A_{op} = A_{pp}$. As is the case for the usual Auger recombination model, it is also assumed that in the elementary collision process, one of the excitons is dissociated via a non-radiative decay process, while the other exciton is regenerated to the $1s$ orthoexcitons and paraexcitons according to their degeneracy, $2n_t \rightarrow \frac{3}{4}n_o + \frac{1}{4}n_p$. The collision-induced spin-flip process¹⁰ from orthoexciton to paraexciton with a cross section C is also included. For simplicity, we assume a constant collision coefficient in the present analysis. According to the conventional model of Auger recombination process, regenerated excitons gain a huge excess energy exceeding the detection range. The orthoexcitons injected by the one-photon phonon-sideband excitation are thermalized after 100 ps, as we reported in a previous work.¹³ Thus we assume that most of the regenerated excitons are observable in the induced absorption spectra. This assumption could lead us to overestimate the A coefficient and underestimate the C coefficient.

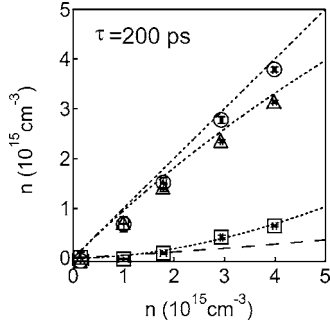


FIG. 4. Densities of ortho (Δ), para (\square), and total (\circ) excitons, measured at a 200 ps pump-probe delay, as a function of the initial exciton density, measured at a 10 ps pump-probe delay. The dotted line shows the calculated density under the collision-induced spin-flip model shown in Eqs. (5) and (6) with a cross section $C=2.6 \times 10^{-16} \text{ cm}^3/\text{ns}$. The broken line shows the paraexciton creation only with the regeneration process by the Auger recombination.

We first discuss the nonlinear paraexciton generation process observed at an early stage, in a high-density excitation regime. Figure 4 shows the densities of the ortho-, para- and total excitons measured at a 200 ps pump-probe delay as a function of the initial density of the orthoexciton, measured at a 10 ps pump-probe delay. With increasing initial density, the ratio of the generated paraexciton density to the total density increases. The total exciton density is approximately proportional to the initial exciton density. This means that, for the ultracold orthoexciton generated via resonant two-photon excitation, the spin-flip process is more important than the dissociation process ($C > A$).²⁸ The early temporal evolutions are analyzed neglecting the linear spin-flip and collision-induced dissociation processes. Equations (3) and (4) turn to

$$\frac{d}{dt}n_p(t) = Cn_o(t)^2, \quad (5)$$

$$n_o(t) + n_p(t) = n_0. \quad (6)$$

By integrating Eq. (5) with Eq. (6) we obtain the density of paraexcitons at a delay time of τ_d as a function of the initial orthoexcitons density n_0 ,

$$n_p(n_0) = \frac{Cn_0^2\tau_d}{1 + Cn_0\tau_d}. \quad (7)$$

We fit the experimental result of n_p at $\tau_d=200$ ps and extract a collision cross section $C=(2.6 \pm 0.1) \times 10^{-16} \text{ cm}^3/\text{ns}$ as shown in Fig. 4. The dotted lines show the calculated densities of the ortho-, para-, and total excitons. The obtained coefficient shows a good agreement with the theoretical value $\tau_{o-p}^{-1} \approx 5[n_o(10^{16} \text{ cm}^{-3})] \text{ ns}^{-1}$.¹⁰ As already mentioned, the value of C was overestimated in our previous paper¹⁹ due to the overlap of the ortho $1s-3p$ components with the para $1s-2p$ signal. The broken line in Fig. 4 shows the expected paraexciton density calculated from the model without a collision-induced spin-flip process assuming an Auger coefficient $A=10^{-16} \text{ cm}^3/\text{ns}$. In that case the paraexciton genera-

tion is much smaller than the experimentally observed values.

Next we consider the high-density excitation at a later stage ($t > 300$ ps). Here, the collision-induced dissociation process can be observed as shown in Fig. 2(d). Assuming that the collision coefficient A is constant, the total exciton density n_t is given by

$$\frac{d}{dt}n_t = -An_t^2. \quad (8)$$

The total density transient following an initial density $n_t(t=0)=n_0$ is

$$n_t(t) = \frac{n_0}{1 + An_0t}. \quad (9)$$

It should be noted that although the theoretical calculation indicate a smaller collision effect for paraexcitons than for orthoexcitons,⁸ we assume for simplicity that the collision coefficient is described by a single coefficient. The temporal evolution of the total exciton density during 0.3–0.8 ns can be reproduced by using Eq. (9). The solid line of Fig. 2(d) shows the calculation of the total exciton density with the collision coefficient $A=10^{-16} \text{ cm}^3/\text{ns}$. The dotted (broken) lines show the numerical calculation of the temporal evolution of orthoexcitons and paraexcitons with (without) collision-induced spin-flip process: $C=2.6 \times 10^{-16} \text{ cm}^3/\text{ns}$, based on the model of Eqs. (3) and (4). The theoretical model with the spin-flip process is in good agreement with the experiments shown in Fig. 2(d). This means that the collision-induced ortho-to-para transformation is important to describe the early stage (< 1 ns) dynamics of excitons after the creation of the supercooled orthoexcitons.

An important question is the paraexciton temperature at a later stage. Although a precise estimate is difficult due to the broad linewidth of the $1s-2p$ paraexciton transition (see Fig. 2), one can nevertheless extract an upper value of 20 K for a pump-probe delay of 800 ps. Such a low temperature cannot be explained assuming a total Auger decay process, where the internal energy of one exciton partner is converted into kinetic energy of the electron and hole of the other partner. On the other hand, the electron spin-exchange process requires an energy of 12 meV to be dissipated. Most of this energy can be emitted in the form of optical phonons with an energy of 9.7 meV. The remaining 2.3 meV should lead to a paraexciton temperature of ~ 25 K. In our opinion, the fact that the paraexcitons are at a lower temperature corresponds to sympathetic cooling of paraexcitons by heat exchange with supercooled orthoexcitons.

We now discuss the feasibility of the excitonic BEC phase. We first estimate the required initial orthoexciton population using the collision cross section $C=2.6 \times 10^{-16} \text{ cm}^3/\text{ns}$ extracted from our data. For A , we take an uppermost value compatible with our results, $A=10^{-16} \text{ cm}^3/\text{ns}$. Assuming an exciton mass $m=2.5-2.7m_e$,¹⁶ a paraexcitons density of $4 \times 10^{16} \text{ cm}^{-3}$ is necessary for excitonic BEC at cryogenic temperature 1.3–1.4 K. Following the calculated temporal evolution of the exciton densities using Eqs. (3) and (4), the initial orthoexcitons with n

$=10^{17} \text{ cm}^{-3}$ give a maximum paraexciton population with a density of $4 \times 10^{16} \text{ cm}^{-3}$ at a 50 ps pump-probe delay. This indicates that the resonant two-photon excitation of orthoexcitons with a density $n=10^{17} \text{ cm}^{-3}$ may be suitable to observe the spontaneous excitonic BEC of paraexcitons. Whether orthoexcitons with a density $n=10^{17} \text{ cm}^{-3}$ are obtained by a resonant two-photon excitation is still not clear because of unknown parameters such as the two-photon absorption coefficient. We need to clarify the optimum excitation condition of the supercooled orthoexcitons. In addition to the conditions of the exciton population, to reach the thermal equilibrium state of paraexcitons at the cryogenic temperature one obviously needs to further cool the paraexcitons to reduce the remaining energy as described in the preceding paragraph. A sympathetic cooling scheme with supercooled orthoexcitons may be available to this end. The supercooled orthoexcitons can play a role of coolant and reduce the paraexcitons' temperature via heat exchange between the supercooled orthoexcitons and hot paraexcitons. Furthermore, we note that the direct Auger recombination process should be strongly dependent on the exciton kinetic energy or the effective temperature since it is caused by a collision process. Indeed, Kavoulakis *et al.*⁸ have theoretically calculated the direct and phonon-assisted Auger recombination coefficient and obtained a much smaller cross section than the present experimental results. To support the present specula-

tion, the temperature dependence of the Auger-like collision effects needs to be clarified.

IV. CONCLUSION

From time-resolved excitonic Lyman spectroscopy under resonant two-photon excitation of orthoexcitons, excitonic collision processes (i.e., dissociation and spin-flip processes) have been investigated quantitatively. As predicted, the collision-induced spin-flip process is dominant over the dissociation process in a supercooled state. A sympathetic cooling scheme with supercooled orthoexciton may then become available. The detailed measurement of the temperature dependence of the Auger-like recombination process and the direct measurement of the unbound electron-hole pair is important for a better understanding of the collision-induced dissociation processes and the stability of the BEC phase.

ACKNOWLEDGMENTS

The authors are grateful to N. Naka and K. Yoshioka for stimulating discussions. The authors also thank J. B. Héroux for a critical reading of this paper. This work is supported in part by a Grant-in-Aid for Scientific Research (S) from the Japan Society for the Promotion of Science.

*Electronic address: gonokami@ap.t.u-tokyo.ac.jp

- ¹J. M. Blatt, K. W. Böer, and W. Brandt, *Phys. Rev.* **126**, 1691 (1962).
- ²*Bose-Einstein Condensation*, edited by A. Griffin, D. W. Snoke, and S. Stringari (Cambridge University Press, Cambridge, 1995).
- ³A. Mysyrowicz, *J. Phys. (Paris)* **41**, 281 (1980).
- ⁴G. M. Kavoulakis, Y.-C. Chang, and G. Baym, *Phys. Rev. B* **55**, 7593 (1997).
- ⁵J. I. Jang, K. E. O'Hara, and J. P. Wolfe, *Phys. Rev. B* **70**, 195205 (2004).
- ⁶K. E. O'Hara, J. R. Gullingsrud, and J. P. Wolfe, *Phys. Rev. B* **60**, 10872 (1999).
- ⁷A. Jolk, M. Jörger, and C. Klingshirn, *Phys. Rev. B* **65**, 245209 (2002).
- ⁸G. M. Kavoulakis and G. Baym, *Phys. Rev. B* **54**, 16625 (1996).
- ⁹J. I. Jang and J. P. Wolfe, *Phys. Rev. B* **72**, 241201(R) (2005).
- ¹⁰G. M. Kavoulakis and A. Mysyrowicz, *Phys. Rev. B* **61**, 16619 (2000).
- ¹¹R. A. Kaindle, M. A. Carnahan, D. Hägele, R. Lövenich, and D. S. Chemla, *Nature (London)* **423**, 734 (2003).
- ¹²R. Huber, R. A. Kaindle, B. A. Schmid, and D. S. Chemla, *Phys. Rev. B* **72**, 161314(R) (2005).
- ¹³M. Kuwata-Gonokami, M. Kubouchi, R. Shimano, and A. Mysyrowicz, *J. Phys. Soc. Jpn.* **73**, 1065 (2004).
- ¹⁴K. Karpinska, P. H. M. van Loosdrecht, I. P. Handayani, and A. Revcolevschi, *J. Lumin.* **112**, 17 (2005).
- ¹⁵M. Jörger, T. Fleck, C. Klingshirn, and R. von Baltz, *Phys. Rev. B*

- 71**, 235210 (2005).
- ¹⁶M. Kuwata-Gonokami, *Solid State Commun.* **134**, 127 (2005).
- ¹⁷T. Tayagaki, A. Mysyrowicz, and M. Kuwata-Gonokami, *J. Phys. Soc. Jpn.* **74**, 1423 (2005).
- ¹⁸M. Kuwata-Gonokami, R. Shimano, and A. Mysyrowicz, *J. Phys. Soc. Jpn.* **71**, 1257 (2002).
- ¹⁹M. Kubouchi, K. Yoshioka, R. Shimano, A. Mysyrowicz, and M. Kuwata-Gonokami, *Phys. Rev. Lett.* **94**, 016403 (2005).
- ²⁰K. Yoshioka and M. Kuwata-Gonokami, *Phys. Rev. B* **73**, 081202(R) (2006).
- ²¹N. Caswell, J. S. Weiner, and P. Y. Yu, *Solid State Commun.* **40**, 843 (1981).
- ²²J. W. Hodby, T. E. Jenkins, C. Schwab, H. Tamura, and D. Trivich, *J. Phys. C* **9**, 1429 (1976).
- ²³G. Dasbach, D. Fröhlich, H. Stolz, R. Klieber, D. Suter, and M. Bayer, *Phys. Rev. Lett.* **91**, 107401 (2003).
- ²⁴M. Y. Shen, T. Yokouchi, S. Koyama, and T. Goto, *Phys. Rev. B* **56**, 13066 (1997).
- ²⁵D. W. Snoke, D. Braun, and M. Cardona, *Phys. Rev. B* **44**, 2991 (1991).
- ²⁶A. Mysyrowicz, D. Hulin, and E. Hanamura, in *Proceedings of the Ultrafast Phenomena VII*, edited by C. B. Harris, E. P. Ippen, G. A. Mourou, and A. H. Zewail, Springer Series in Chemical Physics (Springer, New York, 1990), Vol. 53, p. 245.
- ²⁷A. Jolk, M. Jörger, C. F. Klingshirn, M. Franco, B. Prade, and A. Mysyrowicz, *Phys. Status Solidi B* **221**, 295 (2000).
- ²⁸It is difficult to extract the Auger coefficient precisely from Fig. 4. The upper limit of the Auger coefficient is $A < 10^{-16} \text{ cm}^3/\text{ns}$.